



Biofilm-induced effect on the buoyancy of plastic debris: An experimental study

Paula Núñez^{a,*}, Cristina Misić^b, Laura Cutroneo^b, Marco Capello^b, Raúl Medina^a, Giovanni Besio^c

^a IHCantabria - Instituto de Hidráulica Ambiental de la Universidad de Cantabria, Santander, Spain

^b Dipartimento di Scienze della Terra, dell'Ambiente e della Vita, Università degli Studi di Genova, Corso Europa 26, 16132, Genoa, Italy

^c Dipartimento di Ingegneria Civile, Chimica e Ambientale, Università degli studi di Genova, Via Montallegro 1, 16145 Genoa, Italy

ARTICLE INFO

Keywords:

Plastic debris
Marine pollution
Biofouling
Plastic-debris buoyancy
Terminal velocity

ABSTRACT

Plastic floating on the ocean surface represents about 1 % of all plastic in the ocean, despite the buoyancy of most plastics. Biofouling can help to sink debris, which could explain this discrepancy. A set of laboratory experiments was conducted to investigate biofilm-induced effects on the buoyancy of different plastic debris. Ten materials of different densities (buoyant/non-buoyant), sizes (micro/meso/macro), and shapes (irregular/spherical/cylindrical/flat), including facemasks and cotton swabs, were evaluated. Biofilm was incubated in these materials from a few weeks to three months to investigate the effect of different growth levels on their buoyancy. Biofilm levels and rising/settling velocities were measured and compared at seven time-points. The results show a hindered buoyancy for solid materials, while hollow and open materials showed the opposite trend in early biofilm colonization stages. A relationship was established between biofilm-growth and equivalent sphere diameter that can be used to improve predictive modeling of plastic-debris transport.

1. Introduction

Plastic debris in the marine environment is a growing concern due to its negative impacts on marine life, habitats, and human uses of the ocean (Galvani et al., 2015). Macro (>25 mm), meso (5–25 mm), and microplastics (<5 mm) pose a variety of threats to marine ecosystems, including entanglement, ingestion, transport of invasive species, and habitat modification, and play a significant role in the transport of toxic chemicals (Derraik, 2002; Galloway et al., 2017; Wang et al., 2017; Kühn and Van Franeker, 2020; Ladewig et al., 2023). For this reason, knowledge on the processes that drive plastic-debris transport and dispersion in the marine environment has become an issue of increasing interest in recent times. These processes include the drivers of ocean circulation such as wind, waves, and tides, the intrinsic physicochemical properties of plastic debris, or the biological growth on its surface that modifies these properties and thus its submerged behavior.

Several studies have investigated the behavior of plastic debris numerically at global (Law et al., 2010; Lebreton et al., 2012; Van Sebille et al., 2012; Klink et al., 2022), regional (Kako et al., 2011, 2014; Zambianchi et al., 2014, 2017; Stocchino et al., 2019), and local scales

(Núñez et al., 2019, 2020, 2021), in the latter, paying particular attention to the role of astronomical tide. Field studies have also focused on the presence, abundance, and diffusion mechanisms of plastic debris in local areas (e.g., Mazarrasa et al., 2019; Cutroneo et al., 2020; Chen et al., 2022). These studies have found that plastic debris tends to accumulate in water current convergence zones. Recent experimental studies have also examined the role of waves and wind in the dynamics of micro, meso, and macroplastics in the shoaling zone (where waves transition from deeper to shallower water, increasing their wave height and decreasing wavelength) and in the surf zone (the nearshore region where waves break). In the shoaling zone, buoyant particles are transported toward the coast by Stokes drift, while non-buoyant particles are transported along the seabed by the motion of the wave boundary layer Alsina et al. (2020). In the surf zone, non-buoyant plastic debris shows dominant accumulations in the breaking zone, while buoyant material shows variable accumulation patterns along the coastal profile depending on wind and wave characteristics, as well as debris shape (Alsina et al., 2020; Forsberg et al., 2020; Kerpen et al., 2020; Guler et al., 2022; Larsen et al., 2023; Núñez et al., 2023).

Biofouling growth could alter the findings of plastic-debris transport

* Corresponding author.

E-mail address: nunezp@unican.es (P. Núñez).

<https://doi.org/10.1016/j.marpolbul.2023.115239>

Received 24 May 2023; Received in revised form 26 June 2023; Accepted 29 June 2023

Available online 15 July 2023

0025-326X/© 2023 The Authors. Published by Elsevier Ltd. This is an open access article under the CC BY license (<http://creativecommons.org/licenses/by/4.0/>).

studies such as those mentioned above. Biofouling growth occurs when microorganisms, plants, and animals attach to and grow on the surface of plastic debris and can be divided into microfouling and macrofouling, which are closely related and occur in sequence (Kanematsu and Barry, 2020). Microfouling is caused by bacterial activity. Bacteria, microalgae, and other microorganisms tend to adhere to the surfaces of materials and in turn promote macrofouling, which is caused by the adherence of larger organisms such as barnacles, oysters, etc. Biofouling can significantly alter the physicochemical properties of plastic debris, including its buoyancy, potentially promoting its sinking (Cózar et al., 2014; Eriksen et al., 2014; Kooi, 2017; Lobelle et al., 2021; Fischer et al., 2022). Indeed, recent estimates suggest that the amount of plastic debris floating on the ocean surface represents about 1 % of all plastic in the ocean, despite the buoyancy of most of this material, and biofouling can cause plastic debris to sink and become a more common substrate for marine organisms (Thompson et al., 2009; Andrady, 2011; Subías-Barata et al., 2022). The effect of biofouling on the buoyancy of plastic debris depends on several factors, including the type and amount of fouling material, the density, shape, and size of plastic debris, and the physical properties of the water environment. In general terms, when plastic debris is fouled, its average density increases, which affects its terminal velocity, its transport mode (surface, bottom, or in the water column), and therefore, its distribution and fate (Ye and Andrady, 1991; Morét-Ferguson et al., 2010; Woodall et al., 2014; Chubarenko et al., 2016; Fazey and Ryan, 2016; Halsband, 2021; Fischer et al., 2022; Baudena et al., 2023). If the increase in settling velocity is large, plastic debris may settle near its point of release, probably in the subtidal zone; if the increase is small, plastic debris may travel with currents for the duration of the settling period (Chubarenko et al., 2016; Chubarenko and Stepanova, 2017).

A few studies have experimentally addressed the effect of biofouling on some specific types of plastic debris: buoyant macroplastics, such as six-pack ring material, plastic bags, surgical masks or nitrile gloves (Ye and Andrady, 1991; Misić et al., 2022); two-dimensional (2D) buoyant macro and mesoplastics (Fazey and Ryan, 2016; Chen et al., 2019; Amaral-Zettler et al., 2021), and both buoyant and non-buoyant micropellets (Kaiser et al., 2017; Chen et al., 2019; Miao et al., 2021; Amaral-Zettler et al., 2021; Jalón-Rojas et al., 2022). In addition, Chubarenko et al. (2016) used simplified physical models and geometric considerations to analyze biofouling in microplastics of different densities, shapes, and sizes. The findings of all these studies suggest the following: I) Biofouling responds to a cyclical process. Buoyant macroplastics can be rapidly colonized and eventually sink to the bottom or remain in the water column where defouling and resuspension of the debris occurs (Ye and Andrady, 1991; Misić et al., 2022). II) Whether biofouling can sink debris or not depends on the type of plastic debris, as well as the type of communities developing on its surface (e.g., bacterial colonization is typical of microplastics, while macroorganisms such as blue mussels can grow on larger debris). In general, macroorganisms can cause plastic debris to sink in coastal environments (Ye and Andrady, 1991; Amaral-Zettler et al., 2021); however, if plastic items are too small for macroorganisms to attach, they rarely sink in saltwater (Amaral-Zettler et al., 2021) and can only sink in freshwater through microbial colonization (Chen et al., 2019). III) Finally, Chubarenko et al. (2016) and (Kaiser et al., 2017) investigated a relationship between the size of plastic debris of specific densities and shapes and the colonization time necessary for its sinking. They concluded that the smaller the size of the plastic, the faster it is fouled and reaches the density of water, when it sinks.

While some studies have investigated the influence of biofouling on plastic debris' buoyancy, the magnitude and direction of the effect can vary depending on several factors, such as the type of fouling organisms, plastic-debris' surface properties, and environmental conditions. Therefore, further experimental research is needed to improve these insights into the complex interactions between plastic debris and marine organisms, especially regarding the role of microfouling (Amaral-Zettler

et al., 2021), which would be useful for improving predictive models of plastic debris transport (Fischer et al., 2022).

This study aims to improve the understanding of the biofouling-induced effect, with a focus on microfouling, on the rising/settling terminal velocities (buoyancy) of novel types of plastic debris in still water. A new set of laboratory experiments was performed to assess biofilm growth and its effect on the buoyancy of different types of plastic debris, in terms of density (buoyant and non-buoyant), size (micro, meso, and macrosizes), shape (irregular, spherical, cylindrical, and flat), and flexibility. Hollow cotton swabs and two types of facemasks (surgical and FFP2) were also included due to their significant and increasing presence in the marine environment (Mourgogiannis et al., 2018; De-la Torre and Aragaw, 2021). Biofilm growth was described in terms of increases in carbohydrate accrual per unit of plastic surface area. As for buoyancy, changes in both settling and rising velocities (in the case of buoyant materials), were assessed. Furthermore, the relationship between biofilm growth and its associated changes in equivalent sphere diameter was investigated. This is important because most numerical models designed to predict plastic debris transport and dispersion regard plastics as spherical particles (e.g., Van Sebille et al., 2018; Núñez et al., 2019, 2021; Stocchino et al., 2019; De Leo and Stocchino, 2022).

2. Materials and methods

2.1. Plastic materials

The plastic materials examined in this study were selected from those commonly found in coastal seas, namely: polypropylene (PP: 850–950 kg/m³), low-density polyethylene (LDPE: 900–940 kg/m³), high-density polyethylene (HDPE: 930–990 kg/m³), acrylonitrile butadiene styrene (ABS: 1020–1080 kg/m³), polyamide (PA: 1020–1150 kg/m³), and polyvinylchloride (PVC: 1100–1580 kg/m³) (Zhang, 2017; Mazarrasa et al., 2019; Turner et al., 2020). Polypropylene cotton swabs were also included because this type of debris is still one of the most common debris types found on beaches near wastewater treatment plants (Mourgogiannis et al., 2018). Furthermore, an analysis of facemasks (380–450 kg/m³; Bandi, 2020) was also conducted, as their use has become widespread in recent years due to the global COVID-19 pandemic (De-la Torre and Aragaw, 2021).

Different shapes and sizes of the aforementioned materials were considered, as these characteristics determine their buoyancy, i.e., their position in the water column, and consequently their transport mechanisms and fate (Filella, 2015; Chubarenko and Stepanova, 2017; Zhang, 2017). Shape and specific surface area of debris are also important parameters that determine biofilm processes and can therefore influence the transport pathway of microplastics (Chubarenko et al., 2016; Van Melkebeke et al., 2020). Thus, a total of 10 plastic debris types (hereinafter P_i , $i = 1, \dots, 10$) were analyzed. Fig. 1 and Table 1 gather the main characteristics of these materials, namely: the type of plastic material and its specific density (ρ_p); longest (a), intermediate (b), and shortest (c) axes; average size defined by the nominal diameter ($D_n = \sqrt[3]{a \cdot b \cdot c}$); and shape represented by the dimensionless Corey shape factor ($csf = c/\sqrt{a \cdot b}$), where csf takes values of 1 for perfect spheres and close to 0 for 2D shapes (Corey et al., 1949). Density ρ_p values were obtained from manufacturer information, when available, and from the literature (Zhang, 2017; Bandi, 2020). Test-material sizes were obtained from measurements of at least 20 items of each type, except for P1 and P2, which were provided by the manufacturer. Regarding measurements, the size of the plastic materials was measured with a 0.05 mm resolution caliper and 1 mm resolution graduated scales. The thickness of the flat micromaterials was in all cases provided by the manufacturer.

The analyzed plastic materials have densities ranging from 380 to 970 kg/m³ in buoyant ones (from P1 to P3, P6, and from P8 to P10) and from 1030 to 1340 kg/m³ in non-buoyant ones (P4, P5, and P7). The diameter (D_n) defines microplastics (from P3 to P7), mesoplastics (P1,

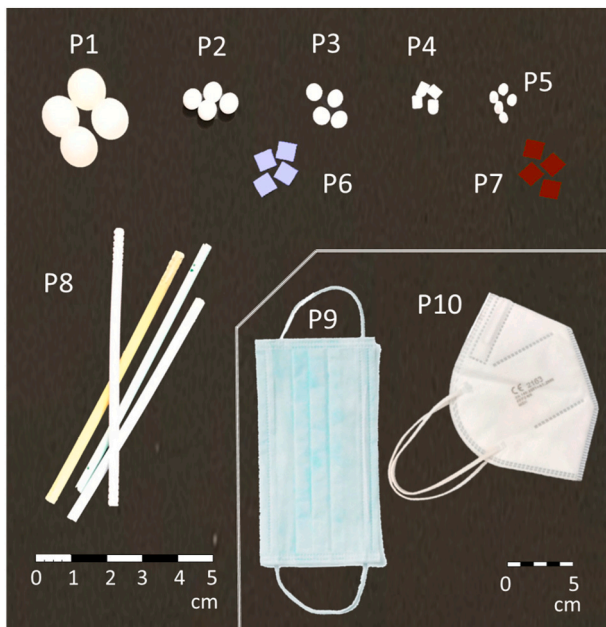


Fig. 1. Plastic materials (P_i) under study. Note the different dimensional scales for P9 and P10 facemasks in relation to the rest of the elements.

P2, and P8), and macroplastics (P9 and P10). Finally, Corey's shape factor (*csf*) defines perfect spheres (P1 and P2), irregular pellets (from P3 to P5), cylindrical (P8), and 2D shapes (P6, P7, P9, and P10).

2.2. Biofilm incubation

Plastic items described in Subsection 2.1 were incubated under controlled laboratory conditions (Amaral-Zettler et al., 2021; Misic et al., 2022) to control biofilm growth and gain insight into the effects of microfouling on plastic debris buoyancy. The incubation process started on September 5th and ended on December 6th, 2022. Samples were collected at six-time points (*t_j*) to investigate the effect of different growth levels on the buoyancy of plastic debris for different time frames (from a few weeks to three months). The 3-month incubation period was chosen to avoid the occurrence of artifacts due to the prolonged laboratory conditions, that are different from those generally found on the field. After this period, 80 % of the studied materials showed a decreasing trend in biofilm accrual, while the remaining 20 % showed a stabilizing trend.

Plastics were immersed in tanks filled with natural seawater (total volume 40 L), collected in the coastal area of Liguria (NW Mediterranean). Seawater showed a density (ρ_w) of approximately 1026 kg/m³ and was kept at a temperature between 19 and 20°C. The lighting was

indirect, artificial, and not particularly intense. Aerators kept the systems oxygenated and in light motion. Biofilm was allowed to grow under natural conditions and under forced conditions, adding inorganic nutrients and organic carbon sources. Assuming that the density of the incubated biofilm remained constant throughout the experiments, its accrual was evaluated by measuring the quantity of polysaccharides adhering on the plastic surfaces (carbohydrate accrual, ρ_{CH} expressed in $\mu\text{g}/\text{cm}^2$). The higher the ρ_{CH} , the greater the development of biofilm (Flemming and Wingender, 2010).

From September 5th to October 24th, plastic materials were immersed in seawater under the natural incubation conditions. Three samples were collected after 2 (t1: September 19th), 4 (t2: October 3rd), and 6 (t3: October 17th) weeks, respectively, to measure terminal velocities.

From October 24th to November 7th, the system was forced by adding inorganic nutrients and glucose to simulate an environment with a higher trophic level. The organic material quickly developed into water and on the plastic materials. A fourth sampling was then carried out (t4: November 7th). The addition of nitrates, orthophosphates (to obtain final concentrations 10 times higher than the normal nutrient concentrations in coastal Ligurian waters: 27 μM for nitrates and 2 μM for orthophosphates, Misic and Covazzi Harriague, 2019), and glucose (final concentration of 0.42 mM, Ylla et al., 2012) led to the relaxation of nutrient and carbon-limitations that are typical of the Ligurian Sea's oligotrophic conditions.

As of November 7th, the remaining materials were subjected to two different treatments. Half of the items were left in the original tank, where only a quarter of the original water volume was left, replacing the other three-quarters with new seawater. In this way, we simulated a system that shows a lower trophic level (less rich in organic matter) maintaining heterotrophic conditions; after two weeks, the fifth sampling was carried out (t5: November 21st). The other half was transferred to a new tank with 100 % clean seawater and was exposed to continuous light (4050 lm, 45 W, red light: 630–660 nm, blue light 450–460 nm) and further nutrient inputs to favor the photoautotrophic component; this period lasted for four weeks after which, the sixth sampling (t6): December 6th, was conducted. Fig. 2 summarizes the incubation process described above.

For each sampling time, carbohydrates were measured following the colorimetric method of DuBois et al. (1956). Briefly, plastic pieces were subjected to sonication (10 min, 40 W power, 40 kHz frequency, Romaní et al., 2004) during the starting phase of the analysis (addition of 5 % phenol), and subsequently the plastic was removed, given that the following addition of concentrated sulfuric acid may cause carbonization/degradation of some plastic types such as masks. Glucose was used as a standard. Absorbance was evaluated at 490 nm with a Jasco V530 spectrophotometer.

Table 1

Main characteristics of the plastic materials under study: specific density (ρ_p); longest (*a*), intermediate (*b*), and shortest (*c*) axes; average size (D_n); Corey shape factor (*csf*), and plastic-debris class. Superscripts (1) and (2) denote values obtained from manufacturer's sources and the literature, respectively. Unsuperscripted values correspond to measurements. Buoyant/non-buoyant materials are denoted by B/NB in the "Class" column.

	Material	ρ_p (kg/m ³)	<i>a</i> (mm)	<i>b</i> (mm)	<i>c</i> (mm)	D_n (mm)	<i>csf</i> (–)	Class
P1	PP	915 ⁽¹⁾	10.0 ⁽¹⁾	10.0 ⁽¹⁾	10.0 ⁽¹⁾	10.0	1.00	Mesosphere/B
P2	PP	915 ⁽¹⁾	5.0 ⁽¹⁾	5.0 ⁽¹⁾	5.0 ⁽¹⁾	5.0	1.00	Mesosphere/B
P3	HDPE	970 ⁽¹⁾	4.7	4.7	2.0	3.5	0.43	Micropellet/B
P4	ABS	1030 ⁽¹⁾	4.0	3.0	2.0	2.9	0.58	Micropellet/NB
P5	PA	1130 ⁽¹⁾	3.0	2.0	1.0	1.8	0.41	Micropellet/NB
P6	LDPE	910 ⁽¹⁾	4.9	4.9	0.07 ⁽¹⁾	1.2	0.01	Microfilm/B
P7	PVC	1340 ⁽¹⁾	4.9	4.9	0.15 ⁽¹⁾	1.5	0.03	Microfilm/NB
P8	PP (cotton swab)	950 ⁽¹⁾	73.0	3.0	3.0	8.6	0.20	Mesoplastic/B
P9	Surgical mask	380 ⁽²⁾	175.0	95.0	1.5	28.4	0.01	Macroplastic/B
P10	FFP2 mask	450 ⁽²⁾	155.0	105.0	2.5	33.5	0.02	Macroplastic/B

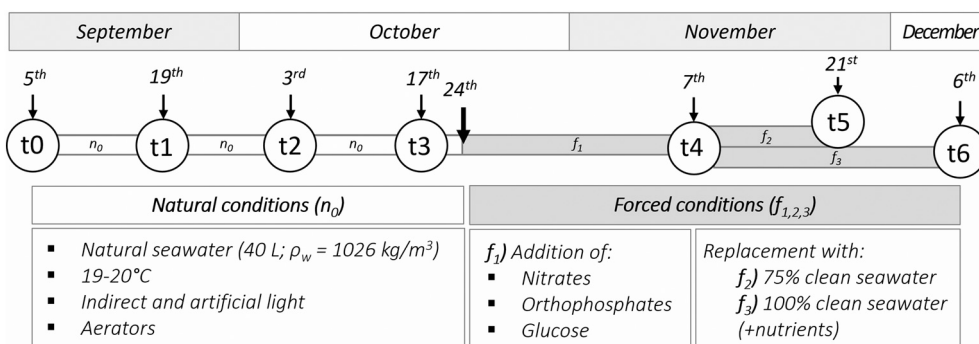


Fig. 2. Timeline of biofilm incubation, including natural (n) and forced (f) experimental conditions, along with corresponding sampling time (t_j).

2.3. Terminal velocity experiments

In order to conduct the terminal velocity experiments, a procedure similar to that used by Kaiser et al. (2017) and Goral et al. (2023) to measure the settling velocity of microplastics was followed but adjusted to measure both rising and settling velocities ($\omega_{r,s}$, where subscripts r and s refer to rising and settling, respectively) of buoyant and non-buoyant plastic materials. Sample material was removed from the incubation tank in water-filled containers (see Fig. 3d) and stored in a refrigerator at 4°C for the duration of the terminal velocity experiments (<12 h) to allow for biofilm preservation and air bubble control. Rising and settling terminal velocities in still water were then evaluated for each plastic material in a $50 \times 50 \times 50 \text{ cm}^3$ tank filled with seawater. The height of the seawater level was set at 48 cm; however, since the tank had a 2 cm platform inside, the effective water height for measuring terminal velocities was 46 cm (Fig. 3a). Terminal velocities were assessed for different biofilm growth conditions: no biofilm growth (t_0) and after each sampling (t_j , $j = 1, 2, \dots, 6$). The effect of the different growth phases was quantified by comparing the velocity measurements in each t_j with respect to t_0 . Density and temperature were the same as those used during incubation (ρ_w around 1026 kg/m^3 and temperature between 19 and 20°C) and were controlled by the “Densito” densimeter (METTLER TOLEDO) which has a precision of 0.001 g/cm^3 (Fig. 3b).

As initial conditions, buoyant materials were deposited at the bottom of the tank using an elongated and smooth element as shown in Fig. 3c. Both facemasks and the cotton swab were placed in a horizontal position

with their shortest dimension, c , perpendicular to the bottom of the tank. Non-buoyant items were placed slightly below the water surface to avoid surface tension effects. Subsequently, the time it took each plastic material to travel through the 46 cm of water column was recorded by a camera. The bottom and top 10 cm being discarded for terminal velocity calculations of the buoyant and non-buoyant materials, respectively. A distance of 10 cm was considered to be sufficient for the various materials to reach their terminal velocities since their movements are likely to occur in a direction perpendicular to the maximum projected area (Stringham et al., 1969; Komar and Reimers, 1978; Middleton and Hampton, 1973; Núñez et al., 2023; Goral et al., 2023) and their thickness was less than 2.5 mm, i.e., 2 orders of magnitude smaller than the 10 cm considered. Preliminary laboratory tests confirmed this assumption.

In this study, a minimum of 40 velocity measurements were taken to determine the mean terminal velocity of each plastic material. For materials P3 to P7, a measurement was made for each item since there were more than 40 items available at each t_j . However, there were only 2 elements at each t_j for materials P1 and P2, 5 for P8, and 3 for P9 and P10, so in these cases, all the available elements for each test material were used to measure the terminal velocities 40 times.

A Canon EOS 40D camera was used to track the positions of the plastics using images taken at a rate of 22 fps and a resolution of 1280×720 pixels. The center point of the camera lens was placed 50 and 26 cm from the front wall and the bottom of the tank, respectively, to cover the entire path of the plastic debris. The terminal velocity of each test material was obtained after calibrating the camera and conducting image

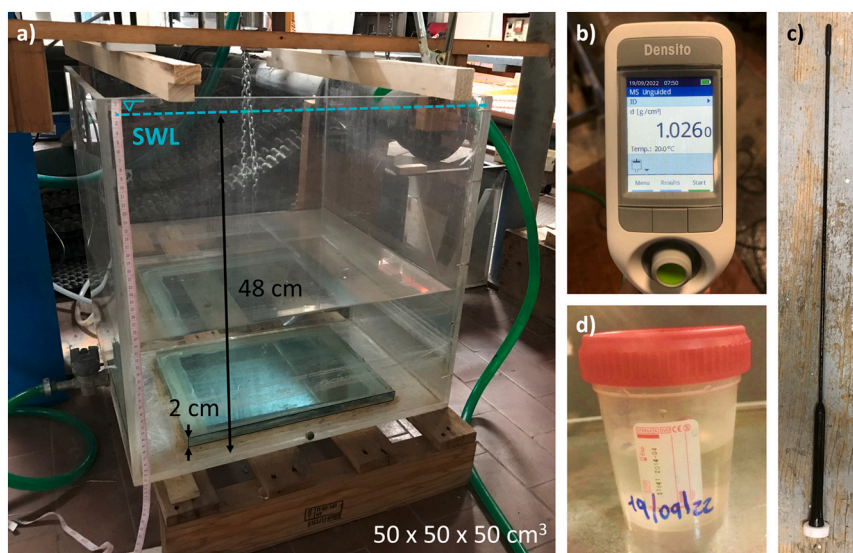


Fig. 3. Experimental setup: a) terminal velocity measurement tank; b) “Densito” densimeter; c) tool for placing buoyant materials at the bottom of the tank; and d) container for sample preservation during the experiments.

post-processing through image analysis techniques based on MATLAB code. Camera calibration ensured accurate spatial mapping by establishing the correspondence between pixel coordinates and real-world dimensions. Image post-processing involved fundamental techniques such as image segmentation, feature extraction, and data analysis, implemented using the capabilities of the MATLAB's Computer Vision Toolbox (MathWorksR, 2021). These techniques allowed for efficient processing and analysis of the images, enabling the accurate determination of the terminal velocity for each test material. Fig. 4 illustrates the ability of the algorithms to identify different sizes of test materials: micropellet P4, cotton swab P8, and surgical facemask P9 and how their terminal velocities are calculated.

2.3.1. Equivalent sphere diameter for numerical applications

The diameter of the sphere with an equivalent terminal velocity to that of each plastic item (D_{eq}) was determined using state-of-the-art formulas (Francalanci et al., 2021, Eq. 1). These formulas relate the terminal velocity (ω) to a reference diameter (D), expressed in a dimensionless way (ω^* and D^* ; Eqs. 2 and 3), and coefficients (C_1 , C_2 , and n), defined as a function of the material's dimensions, i.e., size (a , b , and c) and shape (csf) (Eqs. from 4 to 6).

$$\omega^* = \frac{D^{*2}}{C_1 + (0.75 \cdot C_2 \cdot D^{*3})^n}, \quad (1)$$

$$\omega^* = \left(\frac{\omega}{gR\nu} \right)^{\frac{1}{n}}, \quad (2)$$

$$D^* = D \cdot \left(\frac{gR}{\nu^2} \right)^{\frac{1}{n}}, \quad (3)$$

$$C_1 = 18 \cdot a^{-0.38} \left(\frac{a^2 + b^2 + c^2}{3} \right)^{0.19}, \quad (4)$$

$$C_2 = 0.3708 \cdot csf^{-0.1602}, \quad (5)$$

$$n = 0.4942 \cdot csf^{-0.059}, \quad (6)$$

where g is acceleration due to gravity, R is the submerged relative density of the plastic material defined as $|\rho_w - \rho_p|/\rho_w$, and ν is the kinematic viscosity of water. These formulas were tested and validated for a wide range of plastic shapes (3D, 2D, and 1D) and compositions in quiescent fluids using experimental data and an independent microplastic dataset, such as contributions from the studies by Khatmullina and Isachenko (2017) and Van Melkebeke et al. (2020).

Therefore, knowing the $\omega_{r,s}$ from laboratory measurements and using specific coefficients for spherical particles of the abovementioned formulas (C_1 , C_2 , and n with $a = b = c$; $csf = 1$), D_{eq} can be inferred by applying numerical resolution methods. This diameter can be used to set up numerical models to study plastic debris transport and dispersion.

3. Results

3.1. Biofilm growth

Fig. 5a shows changes in the biofilm level, expressed as changes in the carbohydrate accrual ($\Delta\rho_{CH}$), for each plastic type P_i at each time t_j in which samplings were conducted. Note that this figure does not include the standard deviations for materials P1 and P2 because, as previously mentioned, only 2 samples were available at each time t_j . As an additional limitation, no measurements were available for t_1 , t_3 , t_0 , and t_6 for materials P1, P2, P7, and P9, respectively. However, the 95 % of the total available measurements allowed accurate assessment and interpretation of the results. A detailed overview of the available measurements can be found in the Supplementary Information. For the incubation conditions used in these experiments, the general trend indicates a progressive biofilm growth (fouling process) from the initial time t_0 to t_4 , when the maximum development occurred (although it was a little earlier or later in some materials such as P1, P2, or P9). A decrease in ρ_{CH} (defouling process) was then observed due to the dilution of the concentration of the added substances. An average ρ_{CH} of about $1 \mu\text{g}/\text{cm}^2$ was measured, reaching maximums of about 1.5 and 3.5

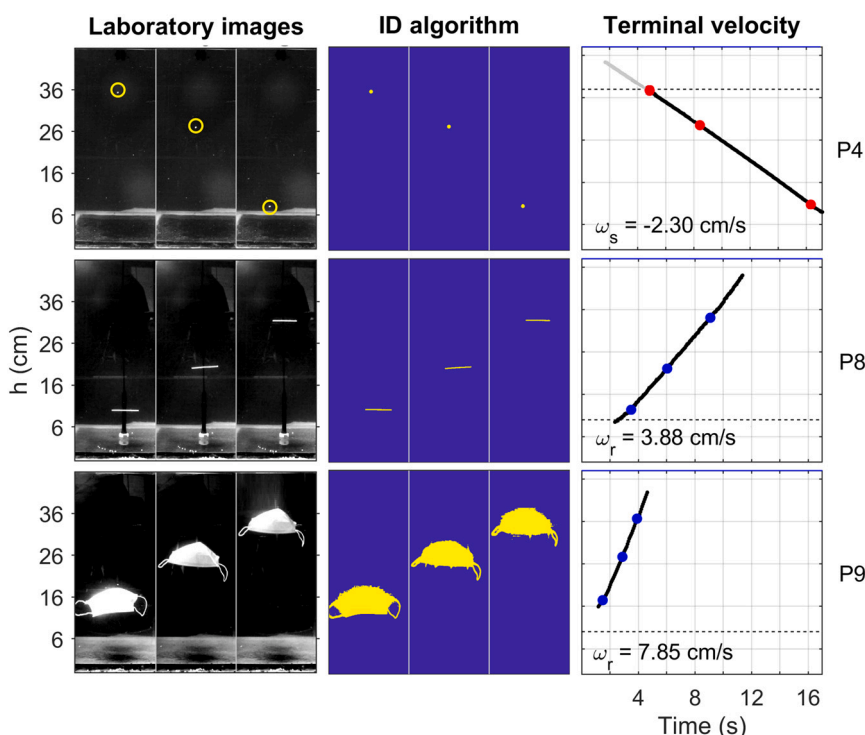


Fig. 4. Results of plastic-debris identification algorithms.

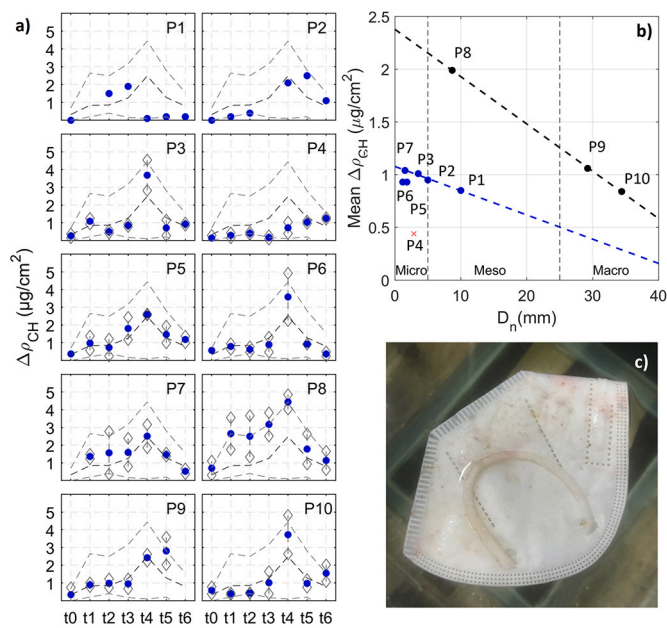


Fig. 5. Biofilm growth in each plastic material (P_i): a) changes in carbohydrate accrual ($\Delta\rho_{CH}$). Blue dots and white diamonds represent the mean change and standard deviation of the accruals, respectively. Dashed gray lines represent the minimum, average, and maximum accrual changes for all 10 types of plastic debris; b) mean biofilm accumulation as a function of D_n ; and c) example of biofilm observed with the naked eye on an FFP2 facemask (P10 plastic material) at t4. (For interpretation of the references to color in this figure legend, the reader is referred to the web version of this article.)

$\mu\text{g}/\text{cm}^2$, for all plastic materials except P8 cotton swabs, which showed the greatest biofilm development. Mean $\Delta\rho_{CH}$ for P8 were close to $2 \mu\text{g}/\text{cm}^2$ and reached $4.5 \mu\text{g}/\text{cm}^2$ at t4.

Panel “b” in Fig. 5 shows the average biofilm development of each material, estimated as the average carbohydrate accumulation during the fouling phase, compared to its nominal diameter. Two main biofilm growth trends were observed. On the one hand, the trend that shows the lower slope describes the behavior of materials from P1 to P7 (although P4 deviates from this behavior), i.e., all non-porous plastic debris (blue dashed line). In this case, a higher biofilm development was observed for 2D shapes or films (such as P7) than for spheres (P1 and P2). On the other hand, a steeper slope was observed for the larger porous materials under study, namely cotton swabs (P8) and facemasks (P9 and P10) (black dashed line). Panel “c” in Fig. 5 shows an example of the large biofilm development observed on P10. All these biofilm trends modified the rising/settling terminal velocities of plastic materials.

3.2. Terminal-velocity changes

3.2.1. Initial terminal velocity

Fig. 6a shows the Probability Density Functions (PDFs) of the terminal velocities of the plastic materials investigated in the laboratory at t0. Median velocities ($\omega_{r,s}^0$) and their corresponding standard deviations (σ) for each P_i are summarized in the first column of Table 2. The standard deviations from the mean value for rigid materials (all P_i except P6, P9, and P10) were always less than 5 %, while flexible materials (P6 microplastic, as well as P9 and P10 facemasks) presented higher deviations, between 7 % and 12 %. Furthermore, it is worth highlighting that some secondary motions were noticed when measuring terminal velocities of macro and mesoplastics. P10 showed the largest secondary movements and P9, the flexible facemask, first rotated its position 180 and then made a vertical ascent to the water’s surface.

The formulas proposed by Francalanci et al. (2021) (see Eqs. from 1

to 6) were used as a cross-check of the measures at t0, with an R^2 of 0.94 (Fig. 6b). Note that these formulas have not been tested yet for large and flexible particles, such as P9 and P10 facemasks. In fact, a relative error of 46 % between the velocities obtained in the laboratory and those resulting from the formulas was obtained for the surgical mask (P9), although this error was only 3 % for the FFP2 facemask (P10). This difference in error may be due to the fact that the surgical mask is more flexible than the FFP2 and therefore its actual projected area in the direction of motion is less than that of the same but more rigid material to which the formulas apply better.

3.2.2. Biofilm influence on terminal velocity

The terminal velocities showed by each plastic at t0 were modified by biofilm growth as shown in Fig. 7. Changes in terminal velocities were observed in response to the fouling and defouling patterns shown in Fig. 5a. In general, except for P8 that showed a peculiar behavior (see below), biofilm growth increased the average density of plastic materials and produced a negative/positive increase in their rising/settling terminal velocities. Positive velocity changes indicate that non-buoyant materials (i.e., P4, P5, and P7) sank or the cotton swab (P8) reached the surface faster following biofilm growth, while negative values indicate that the remaining buoyant materials rose more slowly.

Table 2 summarizes the maximum velocity changes ($\Delta\omega_{r,s}^{max}$) achieved by the biofilm incubated in the materials studied, the minimum biofilm development ($\Delta\rho_{CH}$) required to achieve such a change, and a brief description of the velocity changes observed in each material due to biofilm development. Some plastic types such as P1, P2, P6, P9, and P10 showed the maximum variations in velocity when ρ_{CH} was highest. The P9 surgical mask was the material with the largest change in terminal velocity, decreasing by about 38 % (t4) and 48 % (t5) with biofilm growth. Instead, other plastic types such as P3 and P4, showed a sudden variation in their velocities from t1 onwards, irrespective of the biofilm level colonizing their surface. P5 and P7 showed low variations for all levels of biological development on their surfaces. P8 behaved differently than all the other materials under study. It was the material where the greatest biofilm growth occurred, but this growth increased the rising velocities, contrary to what happened with the rest of the buoyant materials.

The results shown in Fig. 7 and Table 2 suggest that the degree to which biofilm affects the terminal velocities of plastic debris is related also to the intrinsic characteristics of materials, including their size, shape, porosity, and flexibility. This phenomenon is illustrated in Fig. 8, which uses scatter plots and curve fits ($R^2 > 0.75$ and $p < 0.02$ for all materials) to show the degree of velocity change associated with the characteristics of each material for biofilm developments lower than $4 \mu\text{g}/\text{cm}^2$. This biofilm level limit was chosen because it represents the maximum development achieved in these experiments. The material properties are shown in Fig. 8 as follows: buoyant/non-buoyant materials are represented by blue/red colors in panel “a” and solid/dashed lines in panel “b”; markers with different shape and size of panel “b” refer to the shape and size of each plastic material, while *csf* also defines the shape in panel “c”; the porosity is for materials P8, P9, and P10; while the relevant flexibility is for the macroplastic P9.

Sphericity (as described by *cfs*) shows a role in the rates of velocity change. Spherical mesoplastics P1 and P2 (*csf* = 1) showed a gradual velocity change rate from the initial stages of biological growth onwards. These changes were similar, but slightly higher for the element with the smallest diameter, while both rates would increase by 10 % with respect to the initial velocities when carbohydrate density reached values close to $4 \mu\text{g}/\text{cm}^2$. When plastic materials lose sphericity, such as P3, P4, and P5 micropellets (*csf* \approx 0.5), the maximum percentage of velocity change was reached at small increments of biofilm accrual, and the value of this percentage varied for different sizes and compositions of plastic debris. Changes close to 3 %, 12 % and 13 % were achieved for P5 (PA, D_n 1.8 mm), P4 (ABS, D_n 2.9 mm) and P3 (HDPE, D_n 3.5 mm),

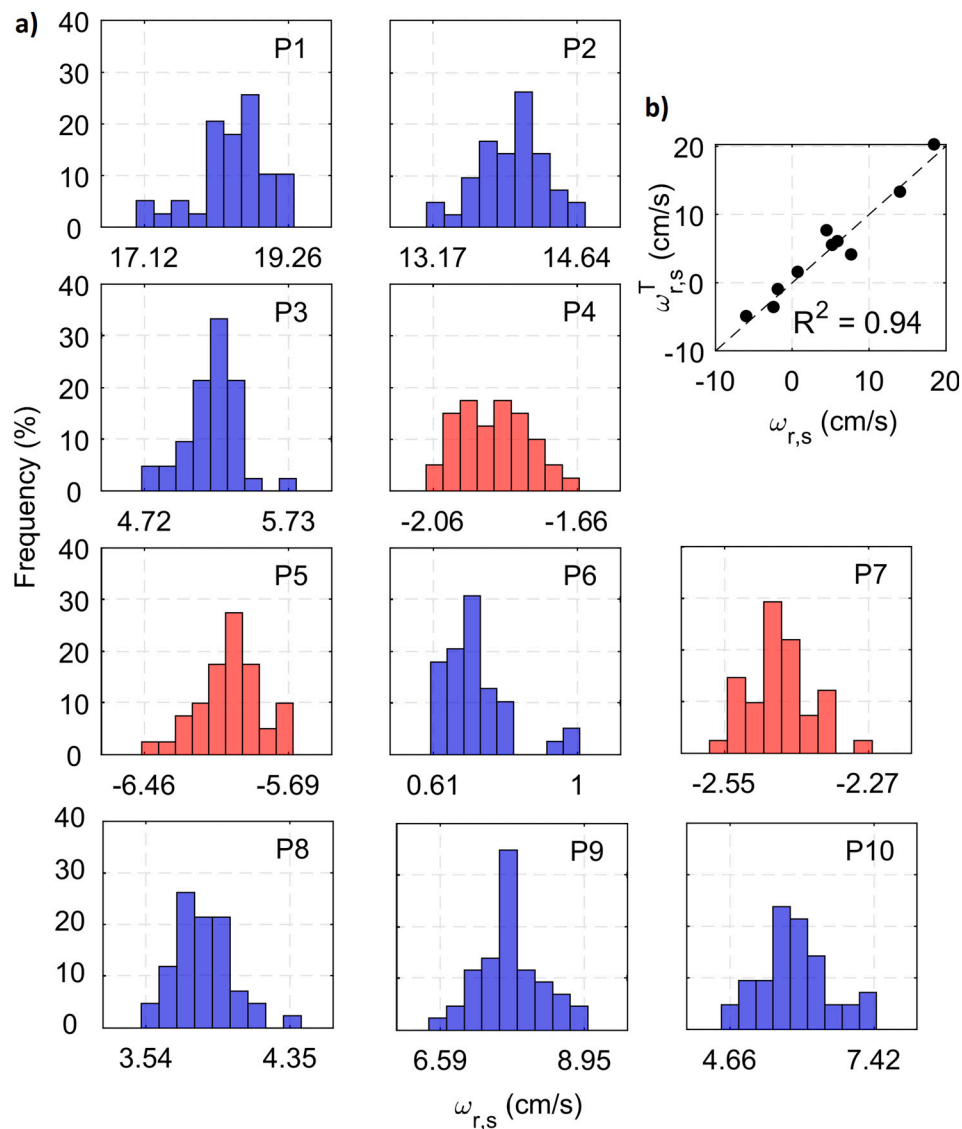


Fig. 6. Experimental terminal velocities ($\omega_{r,s}$, where subscripts r/s refer to rising/settling velocities) at t_0 : a) Probability Density Functions (PDFs) of $\omega_{r,s}$ (blue/red color refers to rising/settling velocities of buoyant/non-buoyant materials) and b) scatter plot between $\omega_{r,s}$ and theoretical estimates ($\omega_{r,s}^T$). (For interpretation of the references to color in this figure legend, the reader is referred to the web version of this article.)

respectively. As mentioned above, the behavior of the cotton swab P8 ($csf \approx 0.2$) was notably different from that of the remaining materials studied, with a 17 % increase in its initial rising velocity for biofilm growths of $4 \mu\text{g}/\text{cm}^2$. For two-dimensional materials, such as microplastics P6 and P7, and facemasks (P9 and P10), there were gradual variations in their terminal velocities, with stronger changes for larger and more flexible elements. With these trends, changes in initial velocity are expected to be about 10 % for P6 and P7, 20 % for the rigid mask P10, and nearly 80 % for the flexible mask P9 for a $\Delta\rho_{CH}$ of $4 \mu\text{g}/\text{cm}^2$.

3.3. Numerical applications

Panels “a” to “d” in Fig. 9 show the dimensionless equivalent diameters related to biofilm level ($D_{eq}^{\Delta\rho_{CH}}$, $\Delta\rho_{CH} = 1, 2, 3,$ and $4 \mu\text{g}/\text{cm}^2$) compared to the initial diameter without biofilm growth (D_{eq}^0). Dashed lines represent the deviations of each $D_{eq}^{\Delta\rho_{CH}}$ from D_{eq}^0 for two-dimensional/three-dimensional microplastics, as well as meso and macroplastics. The R^2 between $D_{eq}^{\Delta\rho_{CH}}$ and such dashed lines was always higher than 0.97. Similar to the changes in terminal velocities (see

Fig. 8), changes in D_{eq}^* were found to depend on debris size, microplastic shape, macroplastic flexibility, and biofilm accrual.

For buoyant materials, except for the hollow and open material P8 (cotton swab), a more profuse biofilm development was associated with a decrease in D_{eq}^* . Average changes of 2 %, 3 %, 5 %, and 7 % were obtained for two-dimensional microplastics (films) with accruals ($\Delta\rho_{CH}$) of 1, 2, 3, and $4 \mu\text{g}/\text{cm}^2$, respectively. Changes from 10 % to 12 % were obtained for three-dimensional microplastics (pellets), while these changes were of 6 %, 10 %, 14 %, and 17 % for meso and macroplastics, except for the large and most flexible material, the P9 surgical facemask, which showed larger changes: 14 %, 30 %, 50 %, and 70 %. According to Eq. 3, the decrease in D_{eq}^* could be achieved by reducing the dimensional diameter or the relative density R of the plastic materials, i.e., by increasing the average density of the buoyant plastic material. During the experiments conducted in this study, the increase in biofilm did not cause significant changes in the size of the plastic materials (since it was microfouling), only affecting their density.

For non-buoyant materials, the percentage of change in the dimensionless diameter obtained was the same as for buoyant materials with the same biofilm growths; however, the dimensionless diameter

Table 2

Influence of incubated biofilm on the buoyancy of plastic materials (P_i): median initial terminal velocities and standard deviations ($\omega_{r,s}^0 \pm \sigma$), maximum changes in terminal velocities ($\omega_{r,s}^{max}$), biofilm development producing such maximum changes ($\Delta\rho_{CH}$), and a brief description of the observed processes. Note that in the first column, positive/negative mathematical signs represent rising/settling velocities, while in the second column, positive/negative signs refer to increases/decreases in the magnitude of terminal velocities, respectively.

	$\omega_{r,s}^0 \pm \sigma$ (cm/s)	$\Delta\omega_{r,s}^{max}$ (%)	$\Delta\rho_{CH}$ ($\mu\text{g}/\text{cm}^2$)	Observations
P1	18.45 ± 0.52	-5 %	>2.0	4 %–5 % reductions in ω_r^0 at t2-t3. These changes coincide with the highest $\Delta\rho_{CH}$ (close to 1.5–2.0 $\mu\text{g}/\text{cm}^2$).
P2	14.02 ± 0.34	-9 %	>2.0	Velocity changes start to be relevant at t3 with $\Delta\rho_{CH}$ around 0.5 $\mu\text{g}/\text{cm}^2$, reducing ω_r^0 by 6 %. Maximum reduction of about 9 % at t4 and maintained at t5 when $\Delta\rho_{CH}$ exceeds 2 $\mu\text{g}/\text{cm}^2$.
P3	5.19 ± 0.19	-13 %	>0.2	13 % reduction in ω_r^0 from t1. Reduction is maintained for the remaining time instants, with $\Delta\rho_{CH}$ ranging from 0.2 to 3.5 $\mu\text{g}/\text{cm}^2$.
P4	-1.89 ± 0.10	10 %	>0.2	10 % positive increase in ω_s^0 from t1, when $\Delta\rho_{CH}$ exceeds 0.2 $\mu\text{g}/\text{cm}^2$.
P5	-6.00 ± 0.17	3 %	>0.4	<3 % change in ω_s^0 regardless of degree of biological development on surface ($\Delta\rho_{CH}$ ranging from 0.4 to 2 $\mu\text{g}/\text{cm}^2$).
P6	0.70 ± 0.09	-7 %	>3.0	No relevant changes in ω_r^0 except at the time of maximum biofilm accrual at t4 ($\Delta\rho_{CH} > 3 \mu\text{g}/\text{cm}^2$), where ω_r^0 decreased by about 7 %.
P7	-2.45 ± 0.06	3 %	>2.0	3 % change in ω_s^0 at t4 when biological development was maximum ($\Delta\rho_{CH}$ close to 2 $\mu\text{g}/\text{cm}^2$).
P8	3.84 ± 0.16	17 %	>4.0	Unlike other buoyant materials, biofilm increased ω_r^0 . 17 % positive increase at the time of maximum biological development ($\Delta\rho_{CH}$ is close to 4 $\mu\text{g}/\text{cm}^2$ at t4).
P9	7.66 ± 0.52	-48 %	>2.5	38 %–48 % reduction in ω_r^0 when $\Delta\rho_{CH}$ was larger than 2 $\mu\text{g}/\text{cm}^2$ (t4) - 2.5 $\mu\text{g}/\text{cm}^2$ (t5).
P10	5.88 ± 0.66	-20 %	>3.0	20 % reduction in ω_r^0 for $\Delta\rho_{CH}$ higher than 3 $\mu\text{g}/\text{cm}^2$ at t4.

increased. In these cases, if the dimensional diameter remained constant, as in our experiments, the relative density should increase and, consequently, the average density of the non-buoyant plastic material must do so too. Nevertheless, in nature, there may also be biological growth that causes additional relevant changes in debris size (Chubarenko et al., 2016).

The dimensionless diameter of the buoyant, hollow, and open meso material P8 showed a similar trend to that of non-buoyant materials. Biofilm growth suggested an increase in the dimensionless diameter but described a different behavior. The initial effective density of the P8 material was a function of the density of the polypropylene and of the water filling the hole. The water gradually encountered more resistance to enter the swab's cavity, being displaced by the development of biofilm, which reduced the initial effective density of this material and therefore increased the relative density and its dimensionless diameter.

All the above percentage changes in D_{eq}^* due to biofilm growth, as well as their trends, are summarized in absolute terms in panel “e” of Fig. 9, where these increments are positive for non-buoyant or buoyant but hollow and open plastic materials, and negative for the remaining buoyant materials.

Obtaining the D_{eq}^* from state-of-the-art formulas requires applying numerical resolution methods. The curve fitting applied to the results of these experiments revealed that there was a relationship between D_{eq}^* , csf , and the dimensionless nominal diameter (D_n^*) of the plastic material, and that this relationship was dependent on the rate of biofilm growth. Panel “f” in Fig. 9 compares the equivalent dimensionless diameters obtained from state-of-the-art formulas ($D_{eq,T}^*$, where subscript T refers to the theoretical approach) and the curve fit ($D_{eq,F}^*$, where subscript F refers to the fit approach) before biofilm growth ($\Delta\rho_{CH} = 0$; black points) and for a range of biofilm growth rates ($\Delta\rho_{CH} = 1, 2, 3$, and 4 $\mu\text{g}/\text{cm}^2$; gray points), with an R^2 of 0.98. This relationship can provide a direct and simple estimate of D_{eq}^* .

4. Discussion

4.1. Biofilm growth

In this study, biofilm was incubated on several types of plastic debris in laboratory facilities to assess how it affects their buoyancy. Previous studies have incubated biofouling on various plastic materials in the field to assess their sinking behavior under different growth rates, including micro and macrofouling. In these studies, biofouling incubation in freshwater (Chen et al., 2019; Miao et al., 2021), coastal waters

(Ye and Andrady, 1991; Fazey and Ryan, 2016; Kaiser et al., 2017; Amaral-Zettler et al., 2021), and estuarine waters (Kaiser et al., 2017) were conducted for time periods in the order of months. Moreover, Amaral-Zettler et al. (2021) and Mistic et al. (2022) incubated microbial biofouling under controlled laboratory conditions for several weeks. Both laboratory and field approaches show pros and cons. Field-based incubations may perfectly replicate real-world environments, but a laboratory approach allows more control over variables such as temperature, salinity, and nutrient levels allowing both reproducibility of the procedures and the forcing of specific processes; it can also minimize contamination from external sources and macrofouling, if required, and the measurement of biofilm may be more accurate in a laboratory setting. Under both approaches, the physical and biochemical conditions of the water (e.g., temperature, availability of nutrients) and the type of plastic debris have been found to be important factors regulating biofilm growth processes.

In general, the biofilm accrual observed in our experiments was in agreement with previous observations (Ye and Andrady, 1991; Mistic et al., 2022). Fluctuations in inorganic nutrient and glucose supply were found to drive biofilm development, showing fouling and defouling phases for all materials (Fig. 5a). Biofilm accrual on each material in terms of quantity of polysaccharides and of time necessary to develop a significant (able to influence terminal velocity of the various items) biofilm matrix was driven by the characteristics of the plastic items. The results of this study show that non-porous plastics host lower average biofilm accruals than porous materials, as described by the two resulting growth trends. For each growth trend, smaller particles accumulated slightly more biofilm than larger debris, which is consistent with previous research such as that of Hidalgo-Ruz et al. (2012) and Chubarenko et al. (2016). Furthermore, the 2D microshapes of P7, showed more biofilm than P1 and P2 spheres, which is also in agreement with the findings of Chubarenko et al. (2016). Cotton swabs, belonging to porous mesoplastics, exhibited the highest biofilm development, probably due to their elongated, hollow, and open shape. All these differences in biofilm accrual may also have been due to the ability of different microbial communities to grow on different plastic types, as shown in previous studies by Zettler et al. (2013), Oberbeckmann et al. (2014), Amaral-Zettler et al. (2020), and Zhou et al. (2021). In fact, P3, P4, and P5 had similar shapes and sphericity, but the development of biofilm was smaller in P4, composed of ABS, than in the other plastic types (HDPE and PA).

4.2. Terminal-velocity changes

Biofilm increased the average density of plastic materials and caused

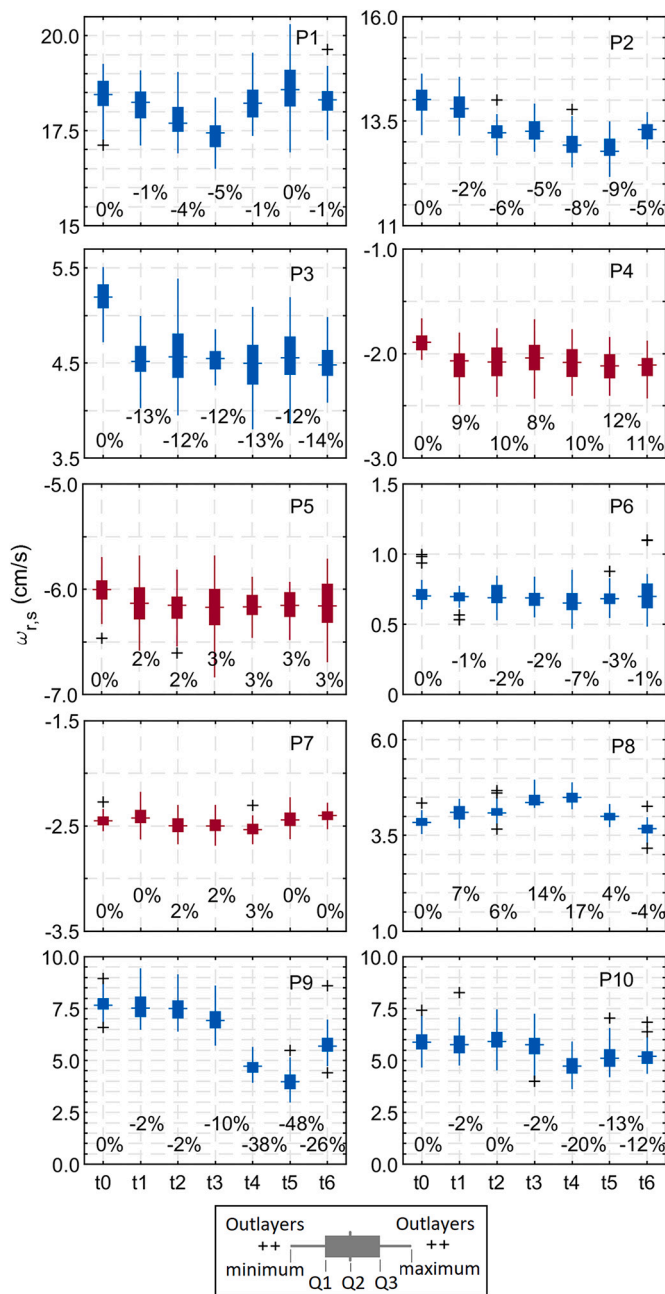


Fig. 7. Evolution of terminal velocity, $\omega_{r,s}$, distributions of each P_i over time (t_j) represented by boxplots (at least 40 repetitions) showing the median (Q2), first and third quartiles (Q1 and Q3), maximum, minimum, and outliers for each distribution; blue/red colors refer to rising/settling velocities of buoyant/non-buoyant materials; numbers within panels indicate the relative increase in median terminal velocity compared to t_0 (no biofilm growth). Note the different scales of the y-axes. (For interpretation of the references to color in this figure legend, the reader is referred to the web version of this article.)

non-buoyant materials to reach the bottom more quickly, and vice versa for buoyant materials, which took longer to rise to the surface (Fig. 7). The exception to this general behavior was shown by cotton swabs, maybe due to the elongated, hollow, and open shape of these items. As described in Section 2, during the velocity measurement experiments, it was ensured that the hollows and pores of the materials were filled with water. In the early stages of the experiments, water would occupy the entire inner hole of P8; however, the development of biofilm took place in both the outer and inner zones of the cotton swab. Thus, the biofilm created a porous media that would gradually hinder water entry to the core of this

material, reducing its average density and increasing its rising velocity.

Field, experimental, or analytical evidence has shown that smaller debris is fouled more quickly and, therefore, sinks faster than larger debris (Hidalgo-Ruz et al., 2012; Chubarenko et al., 2016; Fazey and Ryan, 2016; Van Melkebeke et al., 2020). In this study, microfouling affected the terminal velocities of all the plastics studied but did not cause any of the buoyant materials to sink; nonetheless, it should be born in mind that a change in the exposure conditions (e.g., further nutrient inputs or field incubations) could allow higher biofilm developments or larger organisms to grow on debris, potentially leading to their sinking. This research shows that accumulating the same biofilm level in different types of plastic does not necessarily result in greater changes in the terminal velocities of the smallest debris. It was found that the rates of these changes, assuming constant the density of the biofilm developed on plastic surfaces, are comparable for plastics of similar shape, and that the sign of the change is primarily determined by the specific density of each material and whether it is solid or hollow, while the magnitude of the change appears to be primarily influenced by the size and flexibility of the plastic material. As microparticles lose their sphericity and assume irregular shapes, the maximum rate of change in velocity was reached at smaller increments of biofilm accrual, while the magnitude of this change rate was found to be slightly bigger for larger nominal sizes (a larger surface area implies a larger absolute amount of biofilm in the pellets, which could have a greater impact on their terminal velocities). Similar behaviors were found for macroplastics, with higher rates of change being observed for larger and more flexible materials. However, it should be noted that potential changes in the biofilm density could also affect the buoyancy of plastic elements.

These results thus confirm that the shape, size, and flexibility of plastic debris are significant parameters that strongly affect their terminal velocities and could determine whether biofilm changes their behavior from buoyant to non-buoyant. For instance, if biofilm-induced trends in terminal velocities of buoyant P1, P9, and P10 continue, these materials may eventually sink (see Fig. 8).

4.3. Numerical applications

Numerical models have proven to be an adequate approach to perform comprehensive analyses of the dynamics of plastic debris in different hydrodynamic scenarios (Hardesty et al., 2017). Most of these tools typically use spherical particles to represent debris (e.g., Van Seville et al., 2018; Stocchino et al., 2019; Núñez et al., 2019, 2021; De Leo and Stocchino, 2022); however, plastic debris is often different from a sphere. Thus, key parameters, such as equivalent particle size, which determine transport pathways (e.g., surface, suspension, or bottom) need to be expressed in terms of plastic debris characteristics. Moreover, the explicit description of some processes, such as changes in particle density to account for sinking mechanisms due to biofilm growth, show great scope improvement (Hardesty et al., 2017; Zhang, 2017).

To adequately model the inertial behavior of plastic debris characterized by different shapes, sizes, and densities, it is necessary to identify the diameter of the sphere with an equivalent terminal velocity as the plastic debris of interest. This diameter can be inferred from state-of-the-art formulas (e.g., Dietrich, 1982; Ferguson and Church, 2004; Francalanci et al., 2021; De Leo et al., 2021), once the terminal velocity is known, or by applying the simple approach provided here to quickly estimate this dimensionless diameter taking into account the size and shape of plastic debris (see Fig. 9f). In addition, this study investigated a relationship between biofilm growth and its associated changes in such equivalent diameter, finding different behaviors for 2D microplastics, 3D microplastics, and meso/macroplastics with different flexibilities (see Fig. 9e). All these findings on the relationships between the dimensionless diameter of the equivalent sphere, the characteristics of plastic debris, and the effect of biofilm growth on this dimensionless diameter, can easily be used to set up and improve numerical models of plastic debris transport and dispersion.

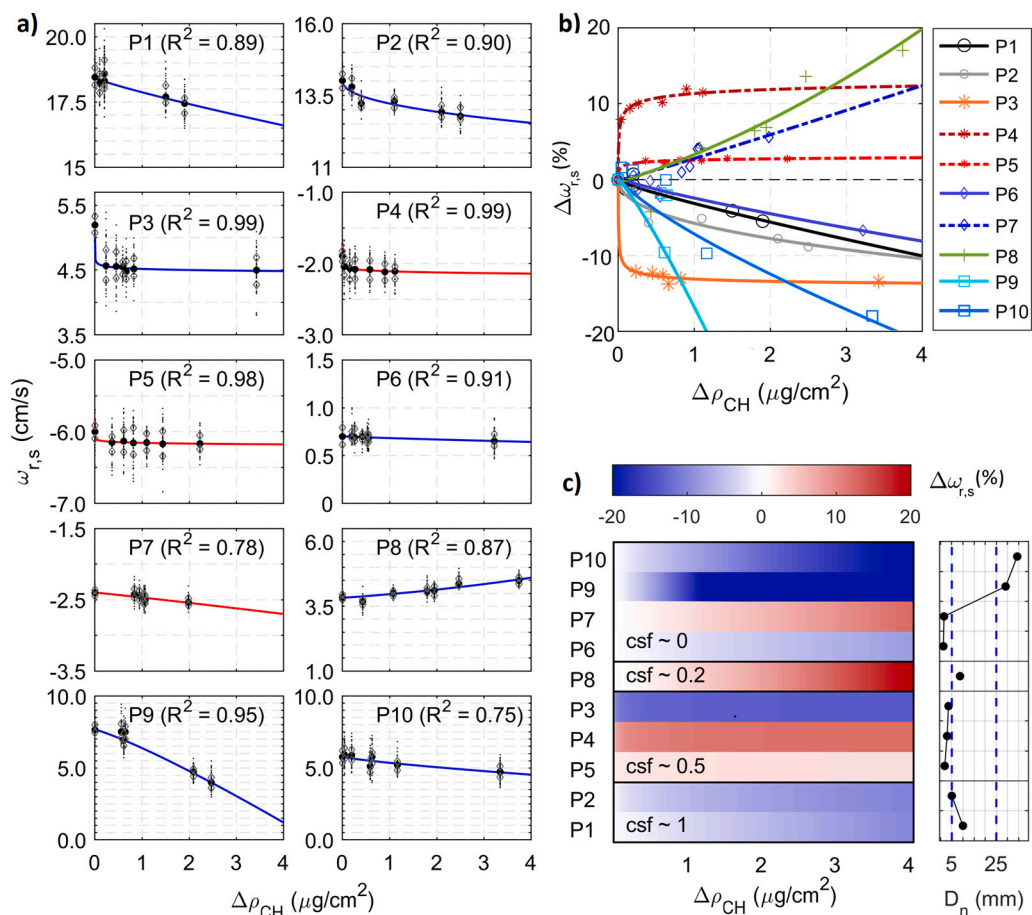


Fig. 8. Terminal velocity as a function of biofilm accumulation ($\omega_{r,s} - \Delta\rho_{CH}$): a) scatter plots and curve fits, where gray/black points represent measured/median velocities and blue/red solid lines refer to buoyant/non-buoyant materials; b) scatter plots and curve fits between changes in velocity, $\Delta\omega_{r,s}$, and $\Delta\rho_{CH}$, where marker size/shape refers to plastic-material size/shape (circle, star, diamond, cross, and square marker shapes refer to sphere, pellet, microfilm, cotton swab, and facemask), marker color shades also group materials by shape (gray/red/blue/green shades for spheres/pellets/2D shapes/cotton swabs), and solid/dashed lines represent buoyant/non-buoyant materials; c) curve-fit matrix plot between $\Delta\omega_{r,s}$ and $\Delta\rho_{CH}$ ordered according to csf (from bottom to top from highest to lowest sphericity) and classified by D_n into micro, meso, and macro sizes (blue dashed lines). (For interpretation of the references to color in this figure legend, the reader is referred to the web version of this article.)

The results of this study complete and expand the existing database in the literature, such as Kaiser et al. (2017); Van Melkebeke et al. (2020), or Jalón-Rojas et al. (2022), on the effect of physical properties of plastic debris and biofouling accumulation on its terminal velocities. Previous studies have focused on the study of microparticles (granules, sheets, and fibers), mainly analyzing sinking velocities and in a few studies, such as Jalón-Rojas et al. (2022), also rising velocities. The present study includes the analysis of rising/settling terminal velocities not only of microplastics, but also of macro/mesoplastics with a current high/increasing presence in the marine environment, such as cotton swabs or facemasks, and several new biological colonization rates. Further research in this direction, including new micro, meso, and macroplastics, is worthwhile to obtain an important extended experimental database for the validation of predictive numerical tools for the transport of plastic debris. Furthermore, it is worth extending these findings to larger biofouling growths when larger organisms such as macroalgae, mollusks, or crustaceans grow on plastic surfaces (Chubarenko et al., 2016) and better understand how these conditions would affect the hydrodynamics around the objects. Water flow around an object can be modified due to processes such as increasing drag and turbulence and cause additional changes in terminal velocity beyond those described in this study. It would also be interesting to study how biofouling alters the terminal velocities of plastic debris of different sizes, shapes, and densities, not only in still water but also under different hydrodynamic conditions. This research topic could be addressed by continuing the study initiated by De Leo et al. (2021) for virgin, or without biofilm growth, spherical microplastic particles exposed to different wave conditions.

5. Conclusions

This research explores the effect of biofilm growth on the terminal velocities of different types of plastic debris. Among the major novelties, the study examines both buoyant and non-buoyant plastic materials, analyzing not only the settling velocities when plastic materials can sink but also changes in rising velocities for buoyant materials. In addition, the study examines plastic materials of various shapes, ranging from perfect spheres to two-dimensional or flat shapes, including hollow and open elements such as cotton swabs. The research also analyzes micro, meso, and macroplastics of various sizes, including flexible surgical facemasks and more rigid FFP2 facemasks as macroplastics.

The biofilm incubated for this study was described in terms of carbohydrate accrual and was found to have a similar average development with slight variations on all plastic materials, except for cotton swabs. Cotton swabs accumulated approximately twice as much biofilm as the other plastic materials, possibly due to their elongated, hollow, and open shape. Considering the slight variations mentioned above, smaller materials showed a higher biofilm development, with non-porous materials revealing a different behavior compared to porous materials. This could be attributed to the fact that different communities can grow on different types of plastic debris.

As microfouling grew in these experiments, no appreciable changes were observed in the size of the analyzed debris, but in their average densities. Microfouling was unable to sink buoyant materials, but it did alter the terminal velocities of all plastic materials analyzed. The general trend indicated an increase in the average density of plastics, resulting in a negative/positive increment in rising/settling velocities of plastic material, limiting their buoyancy. The degree to which biofilm affects the terminal velocities of plastic debris depends strongly on the intrinsic properties of such materials, such as density, size, shape, porosity, or

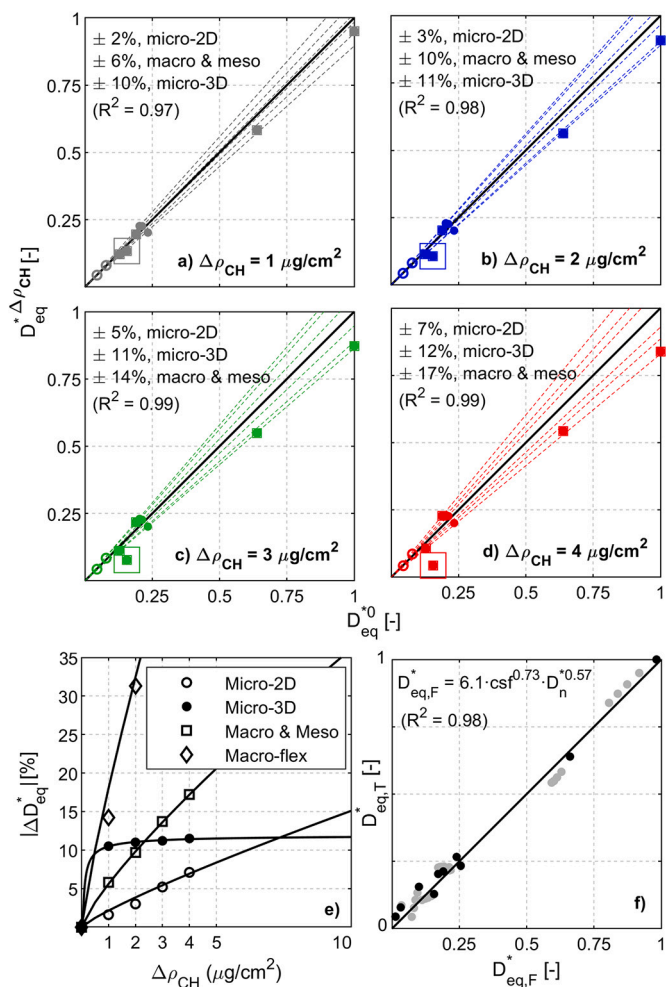


Fig. 9. Changes in the dimensionless diameter of the equivalent sphere (D_{eq}^*) due to the following biofilm growth rates: $\Delta\rho_{CH} = 1$ (a), 2 (b), 3 (c), 4 (d) $\mu\text{g}/\text{cm}^2$. Note that the diameters are standardized between 0 and 1 for the sake of generality. White/solid-color circles represent two-dimensional/three-dimensional microplastics, while solid-color squares represent meso and macroplastics (the flexible surgical mask is highlighted with a larger outer square). Dashed lines represent the deviations caused by biofilm in these diameters with respect to their initial value (without biofilm) for micro-2D, micro-3D, and meso/macroplastic; e) estimates of change in D_{eq}^* , expressed in absolute terms (negative/positive for buoyant/non-buoyant materials), over $\Delta\rho_{CH}$; f) diameter from a theoretical approach, $D_{eq,T}^*$, over diameter from curve fitting, $D_{eq,F}^*$ (black points represent the degree of agreement without biofilm and gray points for the analyzed biofilm rates).

flexibility. Thus, the maximum rate of change for terminal velocities of irregular pellets was achieved with small increments of biofilm accrual, which remained unchanged after the initial change, showing slightly higher rates for the larger sizes. Two-dimensional materials also showed higher rates of change in the largest and most flexible elements, but changes were gradual, progressive, and increased with biofilm growth. Changes were also found to be progressive for perfect spheres; however, the rates of velocity change were similar but slightly higher for the smallest elements. The exception to this general behavior was once again displayed by the cotton swab. Its rising velocity increased in the initial stages of biofilm growth, possibly due to a reduction in effective density caused by biofilm turning it into a porous medium. In short, it was confirmed that the physical characteristics of plastic debris are relevant parameters that strongly influence their terminal velocities and, together with the type of fouling organisms, can determine whether a

specific debris type changes its behavior from buoyant to non-buoyant.

This study increases the available knowledge on a topic of increasing interest: the effect of biofilm on the buoyancy of plastic debris. Our results can be used to improve predictive modeling of plastic-debris transport and dispersion in marine environments. From the obtained results, some relationships and recommendations were provided to fill current gaps in the state-of-the-art numerical modeling of plastic debris transport. It is well-known that the use of spherical particles to represent plastic debris is common in this type of modeling, but plastic debris often has different shapes, such as irregular pellets, films, or fibers. Therefore, it is necessary to define the diameter of the equivalent sphere which travels in the same position in the water column as the plastic debris under study. This diameter can be approximated from state-of-the-art formulas using numerical resolution methods or by applying a more direct and simple relationship provided here between the dimensions and the shape of each debris (see panel “f” of Fig. 9). In addition, some simple relationships have been derived to account for changes due to fouling growth in the density, or where appropriate, the equivalent diameter, of plastic debris with very different physical characteristics (see panel “e” of Fig. 9). In this way, the definition of these key modeling parameters (both the equivalent particle size and change in density or particle size due to biofilm growth) can be addressed. All these insights will aid in the development of more accurate numerical models to study plastic debris and ultimately in the management and mitigation of plastic pollution in marine environments.

CRedit authorship contribution statement

Paula Núñez: Conceptualization, Methodology, Investigation, Data curation, Formal analysis, Writing – original draft, Writing – review & editing, Software, Visualization. **Cristina Misic:** Conceptualization, Methodology, Investigation, Data curation, Funding acquisition, Writing – review & editing. **Laura Cutroneo:** Conceptualization, Funding acquisition, Writing – review & editing. **Marco Capello:** Conceptualization, Funding acquisition, Writing – review & editing. **Raúl Medina:** Conceptualization, Resources, Funding acquisition, Supervision, Writing – review & editing. **Giovanni Besio:** Conceptualization, Resources, Funding acquisition, Supervision, Writing – review & editing.

Declaration of competing interest

The authors declare that they have no known competing financial interests or personal relationships that could have appeared to influence the work reported in this paper.

Data availability

The data are shared as Supplementary Information

Acknowledgements

This work was funded by the European Regional Development Funds (Interreg Maritime IT FR program) under the SPasH & Co project (contract number D35F21002010001). The first author was supported by a Margarita Salas Postdoctoral Fellowship funded by the European Union-NextGenerationEU, Ministry of Universities and Recovery Transformation and Resilience Plan, through a call from the University of Cantabria and the Government of Cantabria through the Fénix program.

Appendix A. Supplementary data

Supplementary data to this article can be found online at <https://doi.org/10.1016/j.marpolbul.2023.115239>.

References

- Alsina, J.M., Jongedijk, C.E., van Sebille, E., 2020. Laboratory measurements of the wave-induced motion of plastic particles: influence of wave period, plastic size and plastic density. *Journal of Geophysical Research: Oceans* 125, e2020JC016294.
- Amaral-Zettler, L.A., Zettler, E.R., Mincer, T.J., 2020. Ecology of the plastisphere. *Nat. Rev. Microbiol.* 18, 139–151.
- Amaral-Zettler, L.A., Zettler, E.R., Mincer, T.J., Klaassen, M.A., Gallagher, S.M., 2021. Biofouling impacts on polyethylene density and sinking in coastal waters: a macro/micro tipping point? *Water Res.* 201, 117289.
- Andrady, A.L., 2011. Microplastics in the marine environment. *Mar. Pollut. Bull.* 62, 1596–1605.
- Bandi, M., 2020. Electrocharged facepiece respirator fabrics using common materials. *Proceedings of the Royal Society A* 476, 20200469.
- Baudena, A., Kiko, R., Jalón-Rojas, I., Pedrotti, M.L., 2023. Low-density plastic debris dispersion beneath the Mediterranean Sea surface. *Environ. Sci. Technol.* 57, 7503–7515.
- Chen, X., Xiong, X., Jiang, X., Shi, H., Wu, C., 2019. Sinking of floating plastic debris caused by biofilm development in a freshwater lake. *Chemosphere* 222, 856–864.
- Chen, Z., Bowen, M., Li, G., Coco, G., Hall, B., 2022. Retention and dispersion of buoyant plastic debris in a well-mixed estuary from drifter observations. *Mar. Pollut. Bull.* 180, 113793.
- Chubarenko, I., Stepanova, N., 2017. Microplastics in sea coastal zone: lessons learned from the Baltic amber. *Environ. Pollut.* 224, 243–254.
- Chubarenko, I., Bagaev, A., Zobkov, M., Esiukova, E., 2016. On some physical and dynamical properties of microplastic particles in marine environment. *Mar. Pollut. Bull.* 108, 105–112.
- Corey, A.T., et al., 1949. Influence of Shape on the Fall Velocity of Sand Grains. Ph.D. thesis. Colorado A & M College.
- Cózar, A., Echevarría, F., González-Gordillo, J.I., Irigoien, X., Úbeda, B., Hernández-León, S., Palma, Á.T., Navarro, S., García-de Lomas, J., Ruiz, A., et al., 2014. Plastic debris in the open ocean. *Proc. Natl. Acad. Sci.* 111, 10239–10244.
- Cutroneo, L., Reboa, A., Besio, G., Borgogno, F., Canesi, L., Canuto, S., Dara, M., Enrile, F., Forioso, I., Greco, G., et al., 2020. Microplastics in seawater: sampling strategies, laboratory methodologies, and identification techniques applied to port environment. *Environ. Sci. Pollut. Res.* 27, 8938–8952.
- De Leo, A., Stocchino, A., 2022. Dispersion of heavy particles under sea waves. *Phys. Fluids* 34, 013305.
- De Leo, A., Cutroneo, L., Sous, D., Stocchino, A., 2021. Settling velocity of microplastics exposed to wave action. *Journal of Marine Science and Engineering* 9, 142.
- De-la Torre, G.E., Aragaw, T.A., 2021. What we need to know about PPE associated with the COVID-19 pandemic in the marine environment. *Mar. Pollut. Bull.* 163, 111879.
- Derraik, J.G., 2002. The pollution of the marine environment by plastic debris: a review. *Mar. Pollut. Bull.* 44, 842–852.
- Dietrich, W.E., 1982. Settling velocity of natural particles. *Water Resour. Res.* 18, 1615–1626.
- DuBois, M., Gilles, K.A., Hamilton, J.K., Rebers, P.T., Smith, F., 1956. Colorimetric method for determination of sugars and related substances. *Anal. Chem.* 28, 350–356.
- Eriksen, M., Lebreton, L.C., Carson, H.S., Thiel, M., Moore, C.J., Borerro, J.C., Galgani, F., Ryan, P.G., Reisser, J., 2014. Plastic pollution in the world's oceans: more than 5 trillion plastic pieces weighing over 250,000 tons afloat at sea. *PLoS One* 9, e111913.
- Fazey, F.M., Ryan, P.G., 2016. Biofouling on buoyant marine plastics: an experimental study into the effect of size on surface longevity. *Environ. Pollut.* 210, 354–360.
- Ferguson, R., Church, M., 2004. A simple universal equation for grain settling velocity. *J. Sediment. Res.* 74, 933–937.
- Filella, M., 2015. Questions of size and numbers in environmental research on microplastics: methodological and conceptual aspects. *Environ. Chem.* 12, 527–538.
- Fischer, R., Lobelle, D., Kooi, M., Koelmans, A., Onink, V., Laufkötter, C., Amaral-Zettler, L., Yool, A., van Sebille, E., 2022. Modelling submerged biofouled microplastics and their vertical trajectories. *BioScience* 19, 2211–2234.
- Flemming, H.C., Wingender, J., 2010. The biofilm matrix. *Nature Reviews Microbiology* 8, 623–633.
- Forsberg, P.L., Sous, D., Stocchino, A., Chemin, R., 2020. Behaviour of plastic litter in nearshore waters: first insights from wind and wave laboratory experiments. *Mar. Pollut. Bull.* 153, 111023.
- Françalanci, S., Paris, E., Solari, L., 2021. On the prediction of settling velocity for plastic particles of different shapes. *Environ. Pollut.* 290, 118068.
- Galgani, F., Hanke, G., Maes, T., 2015. Global distribution, composition and abundance of marine litter. *Marine anthropogenic litter* 29–56.
- Galloway, T.S., Cole, M., Lewis, C., 2017. Interactions of microplastic debris throughout the marine ecosystem. *Nature ecology & evolution* 1, 0116.
- Goral, K.D., Guler, H.G., Larsen, B.E., Carstensen, S., Christensen, E.D., Kerpen, N.B., Schlurmann, T., Fuhrman, D.R., 2023. Settling velocity of microplastic particles having regular and irregular shapes. *Environ. Res.* 115783.
- Guler, H.G., Larsen, B.E., Quintana, O., Goral, K.D., Carstensen, S., Christensen, E.D., Kerpen, N.B., Schlurmann, T., Fuhrman, D.R., 2022. Experimental study of non-buoyant microplastic transport beneath breaking irregular waves on a live sediment bed. *Mar. Pollut. Bull.* 181, 113902.
- Halsband, C., 2021. Effects of biofouling on the sinking behavior of Microplastics in aquatic environments. In: *Handbook of Microplastics in the Environment*. Springer, pp. 1–13.
- Hardesty, B.D., Harari, J., Isobe, A., Lebreton, L., Maximenko, N., Potemra, J., Van Sebille, E., Vethaak, A.D., Wilcox, C., 2017. Using numerical model simulations to improve the understanding of micro-plastic distribution and pathways in the marine environment. *Front. Mar. Sci.* 4, 30.
- Hidalgo-Ruz, V., Gutow, L., Thompson, R.C., Thiel, M., 2012. Microplastics in the marine environment: a review of the methods used for identification and quantification. *Environ. Sci. Technol.* 46, 3060–3075.
- Jalón-Rojas, I., Romero-Ramírez, A., Fauquembergue, K., Rossignol, L., Cachot, J., Sous, D., Morin, B., 2022. Effects of biofilms and particle physical properties on the rising and settling velocities of microplastic fibers and sheets. *Environ. Sci. Technol.* 56, 8114–8123.
- Kaiser, D., Kowalski, N., Waniek, J.J., 2017. Effects of biofouling on the sinking behavior of microplastics. *Environ. Res. Lett.* 12, 124003.
- Kako, S., Isobe, A., Magome, S., Hinata, H., Seino, S., Kojima, A., 2011. Establishment of numerical beach-litter hindcast/forecast models: an application to Goto Islands, Japan. *Mar. Pollut. Bull.* 62, 293–302.
- Kako, S., Isobe, A., Kataoka, T., Hinata, H., 2014. A decadal prediction of the quantity of plastic marine debris littered on beaches of the east Asian marginal seas. *Mar. Pollut. Bull.* 81, 174–184.
- Kanematsu, H., Barry, D.M., 2020. A sequence between microfouling and macrofouling in marine biofouling. *Monit. Artif. Mater. Microbes Marine Ecosyst. Interact. Assess. Methods* 2, 67–80.
- Kerpen, N.B., Schlurmann, T., Schendel, A., Gundlach, J., Marquard, D., Hüppgen, M., 2020. Wave-induced distribution of microplastic in the surf zone. *Front. Mar. Sci.* 7, 590565.
- Khatmullina, L., Isachenko, I., 2017. Settling velocity of microplastic particles of regular shapes. *Mar. Pollut. Bull.* 114, 871–880.
- Klink, D., Peytavin, A., Lebreton, L., 2022. Size dependent transport of floating plastics modeled in the global ocean. *Front. Mar. Sci.* 9, 903134.
- Komar, P.D., Reimers, C., 1978. Grain shape effects on settling rates. *The Journal of Geology* 86, 193–209.
- Kooi, M., Nes, E.H.V., Scheffer, M., Koelmans, A.A., 2017. Ups and downs in the ocean: effects of biofouling on vertical transport of microplastics. *Environ. Sci. Technol.* 51, 7963–7971.
- Kühn, S., Van Franeker, J.A., 2020. Quantitative overview of marine debris ingested by marine megafauna. *Mar. Pollut. Bull.* 151, 110858.
- Ladewig, S.M., Coco, G., Hope, J.A., Vieillard, A.M., Thrush, S.F., 2023. Real-world impacts of microplastic pollution on seafloor ecosystem function. *Sci. Total Environ.* 858, 160114.
- Larsen, B.E., Al-Obaidi, M.A.A., Guler, H.G., Carstensen, S., Goral, K.D., Christensen, E.D., Kerpen, N.B., Schlurmann, T., Fuhrman, D.R., 2023. Experimental investigation on the nearshore transport of buoyant microplastic particles. *Mar. Pollut. Bull.* 187, 114610.
- Law, K.L., Morét-Ferguson, S., Maximenko, N.A., Proskurowski, G., Peacock, E.E., Hafner, J., Reddy, C.M., 2010. Plastic accumulation in the North Atlantic subtropical gyre. *Science* 329, 1185–1188.
- Lebreton, L.M., Greer, S., Borrero, J.C., 2012. Numerical modelling of floating debris in the world's oceans. *Mar. Pollut. Bull.* 64, 653–661.
- Lobelle, D., Kooi, M., Koelmans, A.A., Laufkötter, C., Jongedijk, C.E., Kehl, C., van Sebille, E., 2021. Global modeled sinking characteristics of biofouled microplastic. *Journal of Geophysical Research: Oceans* 126, e2020JC017098.
- MathWorks, 2021. *Computer Vision Toolbox*. Retrieved from <https://www.mathworks.com/products/computer-vision.html>.
- Mazarrasa, I., Puente, A., Núñez, P., García, A., Abascal, A.J., Juanes, J.A., 2019. Assessing the risk of marine litter accumulation in estuarine habitats. *Mar. Pollut. Bull.* 144, 117–128.
- Miao, L., Gao, Y., Adyel, T.M., Huo, Z., Liu, Z., Wu, J., Hou, J., 2021. Effects of biofilm colonization on the sinking of microplastics in three freshwater environments. *J. Hazard. Mater.* 413, 125370.
- Middleton, G.V., Hampton, M.A., 1973. Part I. Sediment Gravity Flows: Mechanics of Flow and Deposition.
- Misic, C., Covazzi Harriague, A., 2019. Development of marine biofilm on plastic: ecological features in different seasons, temperatures, and light regimes. *Hydrobiologia* 835, 129–145.
- Misic, C., Rafael, A., Harriague, A.C., 2022. Organic matter production and recycling in marine biofilm developing on common and new plastics. *Mar. Environ. Res.* 180, 105729.
- Morét-Ferguson, S., Law, K.L., Proskurowski, G., Murphy, E.K., Peacock, E.E., Reddy, C.M., 2010. The size, mass, and composition of plastic debris in the western North Atlantic Ocean. *Mar. Pollut. Bull.* 60, 1873–1878.
- Mourgogiannis, N., Kalavrouziotis, I., Karapanagioti, H., 2018. Questionnaire-based survey to managers of 101 wastewater treatment plants in Greece confirms their potential as plastic marine litter sources. *Mar. Pollut. Bull.* 133, 822–827.
- Núñez, P., García, A., Mazarrasa, I., Juanes, J.A., Abascal, A.J., Méndez, F., Castanedo, S., Medina, R., 2019. A methodology to assess the probability of marine litter accumulation in estuaries. *Mar. Pollut. Bull.* 144, 309–324.
- Núñez, P., Castanedo, S., Medina, R., 2020. A global classification of astronomical tide asymmetry and periodicity using statistical and cluster analysis. *Journal of Geophysical Research: Oceans* 125, e2020JC016143.
- Núñez, P., Castanedo, S., Medina, R., 2021. Role of ocean tidal asymmetry and estuarine geometry in the fate of plastic debris from ocean sources within tidal estuaries. *Estuar. Coast. Shelf Sci.* 259, 107470.
- Núñez, P., Romano, A., García-Alba, J., Besio, G., Medina, R., 2023. Wave-induced cross-shore distribution of different densities, shapes, and sizes of plastic debris in coastal environments: a laboratory experiment. *Mar. Pollut. Bull.* 187, 114561.
- Oberbeckmann, S., Loeder, M.G., Gerdts, G., Osborn, A.M., 2014. Spatial and seasonal variation in diversity and structure of microbial biofilms on marine plastics in northern European waters. *FEMS Microbiol. Ecol.* 90, 478–492.

- Romaní, A.M., Giorgi, A., Acuna, V., Sabater, S., 2004. The influence of substratum type and nutrient supply on biofilm organic matter utilization in streams. *Limnol. Oceanogr.* 49, 1713–1721.
- Stocchino, A., De Leo, F., Besio, G., 2019. Sea waves transport of inertial micro-plastics: mathematical model and applications. *Journal of Marine Science and Engineering* 7, 467.
- Stringham, G.E., Simons, D.B., Guy, H.P., 1969. *The Behavior of Large Particles Falling in Quiescent Liquids*. US Government Printing Office.
- Subías-Barata, A., Sanchez-Vidal, A., Di Martino, E., Figuerola, B., 2022. Marine biofouling organisms on beached, buoyant and benthic plastic debris in the Catalan Sea. *Mar. Pollut. Bull.* 175, 113405.
- Thompson, R.C., Swan, S.H., Moore, C.J., Vom Saal, F.S., 2009. Our Plastic Age. *Turner, A., Arnold, R., Williams, T., 2020. Weathering and persistence of plastic in the marine environment: lessons from LEGO. Environ. Pollut.* 262, 114299.
- Van Melkebeke, M., Janssen, C., De Meester, S., 2020. Characteristics and sinking behavior of typical microplastics including the potential effect of biofouling: implications for remediation. *Environ. Sci. Technol.* 54, 8668–8680.
- Van Sebille, E., England, M.H., Froyland, G., 2012. Origin, dynamics and evolution of ocean garbage patches from observed surface drifters. *Environ. Res. Lett.* 7, 044040.
- Van Sebille, E., Lange, M., Delandmeter, P., 2018. Making Virtual Particles Behave like Plastic: Developing the OceanParcels Lagrangian Ocean Analysis Framework, in: 2018 Ocean Sciences Meeting (AGU).
- Wang, W., Ndungu, A.W., Li, Z., Wang, J., 2017. Microplastics pollution in inland freshwaters of China: a case study in urban surface waters of Wuhan, China. *Sci. Total Environ.* 575, 1369–1374.
- Woodall, L.C., Sanchez-Vidal, A., Canals, M., Paterson, G.L., Coppock, R., Sleight, V., Calafat, A., Rogers, A.D., Narayanaswamy, B.E., Thompson, R.C., 2014. The deep sea is a major sink for microplastic debris. *R. Soc. Open Sci.* 1, 140317.
- Ye, S., Andrady, A.L., 1991. Fouling of floating plastic debris under Biscayne Bay exposure conditions. *Mar. Pollut. Bull.* 22, 608–613.
- Ylla, I., Romaní, A.M., Sabater, S., 2012. Labile and recalcitrant organic matter utilization by river biofilm under increasing water temperature. *Microb. Ecol.* 64, 593–604.
- Zambianchi, E., Iermano, I., Suaria, G., Aliani, S., 2014. Marine litter in the Mediterranean Sea: an oceanographic perspective, in: *Marine litter in the Mediterranean and Black Seas CIESM Workshop Monograph*, CIESM Publisher. pp. 31–41.
- Zambianchi, E., Trani, M., Falco, P., 2017. Lagrangian transport of marine litter in the Mediterranean Sea. *Frontiers in Environmental Science* 5, 5.
- Zettler, E.R., Mincer, T.J., Amaral-Zettler, L.A., 2013. Life in the “plastisphere”: microbial communities on plastic marine debris. *Environ. Sci. Technol.* 47, 7137–7146.
- Zhang, H., 2017. Transport of microplastics in coastal seas. *Estuar. Coast. Shelf Sci.* 199, 74–86.
- Zhou, Y., Kiely, P.D., Kibbee, R., Ormeci, B., 2021. Effect of polymeric support material on biofilm development, bacterial population, and wastewater treatment performance in anaerobic fixed-film systems. *Chemosphere* 264, 128477.